Bilinear Hyperspectral Unmixing via Tensor Decomposition

Meng Ding
School of Math.
Southwest Jiaotong Univ.
Chengdu, China

Xiao Fu
School of Elec. Eng. & Computer Sci.
Oregon State Univ.
Corvallis, OR 97331, United States

Xi-Le Zhao
School of Math. Sci.
Univ. of Elec. Sci. & Tech. of China
Chengdu, China

Abstract—The *bilinear mixture model* (BMM) is often used in hyperspectral unmixing (HU) for incorporating nonlinear effects, which is considered more general than the widely used linear mixture model (LMM). Existing BMM-based HU methods often lack identifiability guarantees of the endmembers and their abundances unless some stringent conditions are met. This work puts forth a new framework for BMM-based HU. Our method models the hyperspectral image as a latent factor-structured block-term tensor decomposition model with multilinear rank-$(L_r, L_r, 1)$ terms ("LL1" model for short). This way, the HU task boils down to finding the block terms of the tensor model. The LL1 model's essential uniqueness naturally provides identifiability guarantees of the endmembers/abundances under reasonably mild conditions. An alternating *gradient projection* (GP) algorithm is proposed to takle the formulated tensor decomposition-based BMM-HU problem. Simulations on semi-real and real datasets show the high-quality unmixing performance of the proposed GP algorithm compared to state-of-the-art methods.

Index Terms—Bilinear hyperspectral unmixing, block-term tensor decomposition, identifiability

I. INTRODUCTION

Hyperspectral unmixing (HU) techniques estimate the endmembers and their corresponding proportions (abundances) from the high-dimensional pixels. The pixels are often mixtures of the endmembers due to low spatial resolution of the hyperspectral sensors [1], [2]. The widely used *linear mixture model* (LMM) expresses a pixel as the convex combination of the endmembers [2]. Nonetheless, the LMM could be overly simplified as nonlinearity oftentimes arises in hyperspectral image (HSI). Efforts have been made towards fending against nonlinearity in HU via using various nonlinear models; see, e.g., [3]. Among these nonlinear models, the *bilinear mixture model* (BMM) is arguably one of the most widely adopted due to its effectiveness in capturing sunlight reflection among more than one material [4]–[8].

Over the past decade, many BMM algorithms were developed; see, e.g., [4]–[8]. However, most of the existing BMM models lack identifiability guarantees of the endmembers and their abundances. The recent works [9], [10] studied and established the identifiability for BMM-based HU. Nevertheless,

the identifiability only holds under some relatively stringent conditions, e.g., the pure pixel condition and its variants. But such conditions are not always easy to meet.

In this work, we propose a new BMM-based HU algorithm from a tensor decomposition perspective. We model the hyperspectral images as a block-term tensor decomposition model with multilinear rank-$(L_r, L_r, 1)$ terms ("LL1" model for short). This way, estimating the abundances and the endmembers boils down to recovering the block terms of the LL1 tensor model. One of the advantages of adopting this perspective is that the LL1 decomposition allows for the identification of block terms under relatively mild conditions, which aligns well with the objectives of HU. Computing the LL1 decomposition under constraints arising in the context of BMM-based HU is highly nontrivial. We develop an alternating *gradient projection* (GP) algorithm and a heuristic *alternating projection* (AP) solver to handle the challenging structural constraints. Simulations show that the proposed algorithm produces more accurate results for estimating both linear and bilinear abundances relative to state-of-the-art methods.

II. BACKGROUND

A. BMM-based HU

Consider a HSI $\underline{\boldsymbol{Y}} \in \mathbb{R}^{I \times J \times K}$, where I and J denote the vertical and horizontal spatial dimensions, respectively, and K is the spectral dimension. A vector $\boldsymbol{y}_\ell := \underline{\boldsymbol{Y}}(i, j, :) \in \mathbb{R}^K$, $(i = 1, \ldots, I, \ j = 1, \ldots, J)$ represents a K-dimensional hyperspectral pixel, in which we have

$$\ell = I(j - 1) + i.$$

If the noise is absent, the BMM for $\boldsymbol{y}_\ell$ is expressed as follows [11]:

$$\boldsymbol{y}_\ell = \boldsymbol{C}\boldsymbol{s}_\ell + \sum_{r=1}^{R-1} \sum_{m=r+1}^{R} e_\ell^{r,m} \boldsymbol{c}_r \odot \boldsymbol{c}_m$$
$$= \boldsymbol{C}\boldsymbol{s}_\ell + \widetilde{\boldsymbol{C}}\boldsymbol{e}_\ell, \tag{1}$$

where $\boldsymbol{C} = [\boldsymbol{c}_1, \ldots, \boldsymbol{c}_R] \in \mathbb{R}^{K \times R}$ contains R endmembers' spectral signatures (i.e., $\boldsymbol{c}_r \in \mathbb{R}^K$, $r = 1, \ldots, R$), and the corresponding abundance vector $\boldsymbol{s}_\ell \in \mathbb{R}^R$ satisfies the following simplex constraint [1], [2] under the physical mechanism:

$$\mathbf{1}^\top \boldsymbol{s}_\ell = 1, \ \boldsymbol{s}_\ell \geq \mathbf{0}, \ \ell = 1, \ldots, IJ, \tag{2}$$
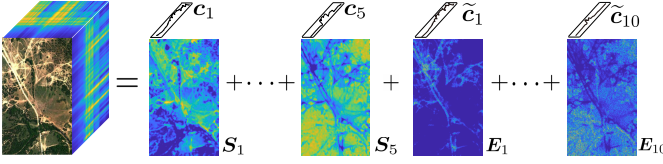
Fig. 1. Illustration of the bilinear HU.

Fig. 2. Illustration of the LL1 model.

where $\mathbf{1}$ is an all-1 vector with a proper length, and $s_{r,\ell}$ is the proportion of r-th endmember in the pixel ℓ. The term $\boldsymbol{C}\boldsymbol{s}_\ell$ is the same as the LMM for HSI [1]. The additional term $\widetilde{\boldsymbol{C}}\boldsymbol{e}_\ell$ is called the bilinear mixture term, which models the reflections between two different endmembers that is considered as a major source of nonlinearity in HSI acquisition. Note that $e_\ell^{r,m} \in [0,1]$ stands for the abundance of the "virtual endmember" $\boldsymbol{c}_r \odot \boldsymbol{c}_m$ that is created by the reflections between endmembers r and m, where $\odot$ is the Hadamard (element-wise) product. The matrix $\widetilde{\boldsymbol{C}} \in \mathbb{R}^{K \times P}$ $(P = (R-1)R/2)$ denotes the bilinear virtual spectral signatures, i.e.,

$$\widetilde{\boldsymbol{C}} = [\boldsymbol{c}_1 \odot \boldsymbol{c}_2, \ldots, \boldsymbol{c}_1 \odot \boldsymbol{c}_R, \boldsymbol{c}_2 \odot \boldsymbol{c}_3, \ldots, \boldsymbol{c}_{R-1} \odot \boldsymbol{c}_R],$$

and $\boldsymbol{e}_\ell = [e_\ell^{1,2}, \ldots, e_\ell^{1,R}, e_\ell^{2,3}, \ldots, e_\ell^{R-1,R}]^\top$ is the abundance vector associated with bilinear endmembers.

Putting all pixels together $\boldsymbol{Y} = [\boldsymbol{y}_1, \ldots, \boldsymbol{y}_{IJ}] \in \mathbb{R}^{K \times IJ}$, the HSI can be expressed as follows:

$$\boldsymbol{Y} = \boldsymbol{C}\boldsymbol{S} + \widetilde{\boldsymbol{C}}\boldsymbol{E}, \tag{3}$$

where $\boldsymbol{S} = [\boldsymbol{s}_1, \ldots, \boldsymbol{s}_{IJ}] \in \mathbb{R}^{R \times IJ}$, and $\boldsymbol{E} = [\boldsymbol{e}_1, \ldots, \boldsymbol{e}_{IJ}] \in \mathbb{R}^{P \times IJ}$. Reshaping $\boldsymbol{Y}$ into a third-order tensor, we have

$$\underline{\boldsymbol{Y}} = \sum_{r=1}^{R} \boldsymbol{S}_r \circ \boldsymbol{C}(:,r) + \sum_{p=1}^{P} \boldsymbol{E}_p \circ \widetilde{\boldsymbol{C}}(:,p), \tag{4}$$

where $\boldsymbol{C}(:,r) = \boldsymbol{c}_r$, $\circ$ denotes the outer product, and $\widetilde{\boldsymbol{C}}(:,p) = \boldsymbol{c}_r \odot \boldsymbol{c}_m$ with $p = m - r + \sum_{\tilde{r}=1}^{r-1}(R - \tilde{r})$ $(1 \leq r < m \leq R)$, the matrix $\boldsymbol{S}_r \in \mathbb{R}^{I \times J}$ is the *abundance map* of the rth endmember, which can be obtained by reshaping the rth row vector $\boldsymbol{S}(r,:) \in \mathbb{R}^{IJ}$, i.e.,

$$\boldsymbol{S}(r,:) = \mathrm{vec}(\boldsymbol{S}_r)^\top,$$

where the $\mathrm{vec}(\cdot)$ is the "vectorization" operator. Also, we can get the pth bilinear abundance map $\boldsymbol{E}_p$ via $\boldsymbol{E}(p,:) = \mathrm{vec}(\boldsymbol{E}_p)^\top$. The signal model in (4) is illustrated in Fig. 1.

The linear abundance maps satisfy the simplex constraint $\sum_{r=1}^{R} \boldsymbol{S}_r = \mathbf{1}\mathbf{1}^\top$ and $\boldsymbol{S}_r \geq \mathbf{0}$. The goal of BMM-based HU is to find $\boldsymbol{S}$, $\boldsymbol{C}$, and $\boldsymbol{E}$ simultaneously.

B. Existing BMM Methods

Under the matrix formulation in (3), a large number of matrix-based methods have been proposed for bilinear HU, please see more introductions in [3], [11] and references therein. As a blind source separation problem, the identifiability of $\boldsymbol{C}$, $\boldsymbol{S}$, and $\boldsymbol{E}$ in (3) plays an important role in the effectiveness of the bilinear HU. However, the identifiability of BMM-based HU has been less studied until recent works [9], [10], which both require the factors $\boldsymbol{C}$, $\boldsymbol{S}$, and $\boldsymbol{E}$ satisfying
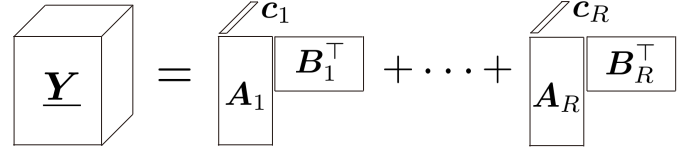
certain conditions. To be specific, the work in [9] relied on two strong assumptions: (1) the abundance map $[\boldsymbol{S}; \boldsymbol{E}]$ has full row rank, and all possible interactions of two endmembers must be present in the HSI; (2) the wavelength K of HSI should be of the order $K \approx O(R^4)$. The identifiability condition in [10] requires the existence of the pure pixels, which is often used in LMM-based HU [12], [13]. However, these conditions are relatively stringent and may not always hold.

C. LL1 *Tensor Decomposition*

In this work, we will tackle the BMM-based HU problem from an LL1 tensor decomposition viewpoint. The LL1 model (see Fig. 2) decomposes a third-order tensor $\underline{\boldsymbol{Y}} \in \mathbb{R}^{I \times J \times K}$ into the sum of a set of latent components, in which each component is expressed as the outer product of a vector and a low-rank matrix. To be specific, we have

$$\underline{\boldsymbol{Y}} = \sum_{r=1}^{R} (\boldsymbol{A}_r \boldsymbol{B}_r^\top) \circ \boldsymbol{C}(:,r), \tag{5}$$

where $\boldsymbol{A}_r \in \mathbb{R}^{I \times L_r}$, $\boldsymbol{B}_r \in \mathbb{R}^{J \times L_r}$, and $\boldsymbol{C} \in \mathbb{R}^{K \times R}$. The LL1 model in (5) has an important identifiability property:

Theorem 1 ([14])**.** *Assume that the latent factors $(\boldsymbol{A}_r, \boldsymbol{B}_r, \boldsymbol{C})$ in (5) are drawn from any joint absolutely continuous distributions. Assume that $L_r = L$, the LL1 decomposition of $\underline{\boldsymbol{Y}}$ is essentially unique almost surely if $IJ \geq L^2 R$, and*

$$\min\left(\left\lfloor \frac{I}{L} \right\rfloor, R\right) + \min\left(\left\lfloor \frac{J}{L} \right\rfloor, R\right) + \min(K, R) \geq 2R + 2.$$

Here, the term "essential uniqueness" means that if we have $(\bar{\boldsymbol{A}}_r, \bar{\boldsymbol{B}}_r, \bar{\boldsymbol{C}})$ satisfying $\underline{\boldsymbol{Y}} = \sum_{r=1}^{R} (\bar{\boldsymbol{A}}_r(\bar{\boldsymbol{B}}_r)^\top) \circ \bar{\boldsymbol{C}}(:,r)$, there must exist a permutation matrix $\boldsymbol{\Pi}$ and a nonsingular diagonal matrix $\boldsymbol{\Lambda}$ such that $\bar{\boldsymbol{S}} = \boldsymbol{S}\boldsymbol{\Pi}\boldsymbol{\Lambda}$, $\bar{\boldsymbol{C}} = \boldsymbol{C}\boldsymbol{\Pi}\boldsymbol{\Lambda}^{-1}$, where $\bar{\boldsymbol{S}} = [\mathrm{vec}(\bar{\boldsymbol{S}}_1), \ldots, \mathrm{vec}(\bar{\boldsymbol{S}}_R)]^\top$, $\bar{\boldsymbol{S}}_r = \bar{\boldsymbol{A}}_r(\bar{\boldsymbol{B}}_r)^\top$, $\boldsymbol{S} = [\mathrm{vec}(\boldsymbol{S}_1), \ldots, \mathrm{vec}(\boldsymbol{S}_R)]^\top$, and $\boldsymbol{S}_r = \boldsymbol{A}_r \boldsymbol{B}_r^\top$.

Note that due to the important identifiability property, the LL1 model has been successfully employed for many tasks, e.g., LMM-based HU [15], [16], hyperspectral super-resolution [17], and spectrum cartography in wireless communications [18].

III. LL1-BASED BILINEAR HU

The spread of each material over the spatial domain often exhibits high correlation across neighboring pixels. Hence, the abundance maps $\boldsymbol{S}_r$ can be approximated by low-rank matrices—as observed in the LMM works [15]–[17]. Using

the same idea to model $\boldsymbol{E}_p$, we assume that the following hold:

$$\text{rank}(\boldsymbol{S}_r) \leq L_r \quad \text{and} \quad \text{rank}(\boldsymbol{E}_p) \leq Q_p. \tag{6}$$

Therefore, the model (4) can be re-written as

$$\underline{\boldsymbol{Y}} = \sum_{r=1}^{R} (\boldsymbol{A}_r \boldsymbol{B}_r^\top) \circ \boldsymbol{C}(:,r) + \sum_{p=1}^{P} (\boldsymbol{M}_p \boldsymbol{N}_p^\top) \circ \widetilde{\boldsymbol{C}}(:,p), \tag{7}$$

where $\boldsymbol{A}_r \in \mathbb{R}^{I \times L_r}$, $\boldsymbol{B}_r \in \mathbb{R}^{J \times L_r}$, $\boldsymbol{S}_r = \boldsymbol{A}_r \boldsymbol{B}_r^\top$, $\boldsymbol{M}_p \in \mathbb{R}^{I \times Q_p}$, $\boldsymbol{N}_p \in \mathbb{R}^{J \times Q_p}$, and $\boldsymbol{E}_p = \boldsymbol{M}_p \boldsymbol{N}_p^\top$. The model in (7) is clearly an LL1 model. Hence, by applying Theorem 1, one can obtain the following identifiability guarantee immediately:

Fact 1. *Assume that the latent factors $\boldsymbol{A}_r$, $\boldsymbol{B}_r$, $\boldsymbol{M}_p$, $\boldsymbol{N}_p$, and $\boldsymbol{C}$ in (7) are drawn from any absolutely continuous distributions. Then, the bilinear LL1 decomposition of $\underline{\boldsymbol{Y}}$ is essentially unique almost surely, if $L_r = L$, $Q_p = Q$, $O = \max(L, Q)$, $IJ \geq \max\left(L^2 R,\ Q^2 R\right)$ and*

$$\min\left(\left\lfloor \frac{I}{O} \right\rfloor, \frac{R(R+1)}{2} \right) + \min\left(\left\lfloor \frac{J}{O} \right\rfloor, \frac{R(R+1)}{2} \right)$$
$$+ \min(K, R(R+1)) \geq 2R(R+1) + 2.$$

Note that the identifiability result does not require $K \approx O(R^4)$ as in [9]. Instead, $K \approx O(R^2)$ is enough. In addition, unlike [10], there is no requirement for the existence of pure pixels. Hence, the LL1 tensor decomposition perspective offers a valuable alternative to existing identifiability-ensured BMM HU toolkit, covering scenarios where the existing approaches could not provide identifiability guarantees.

A. Constrained LL1 for bilinear HU

To proceed, we propose the following tensor decomposition criterion:

$$\min_{\boldsymbol{S},\boldsymbol{C},\boldsymbol{E}} \frac{1}{2} \left\| \boldsymbol{Y} - \boldsymbol{C}\boldsymbol{S} - \widetilde{\boldsymbol{C}}\boldsymbol{E} \right\|_F^2 + \theta_1 \varphi(\boldsymbol{S}) + \theta_2 \varphi(\boldsymbol{E}) \tag{8a}$$

$$\text{s.t. } \boldsymbol{S}_r \in \mathcal{A}_{\text{LR}}, \ r = 1, \ldots, R, \tag{8b}$$

$$\boldsymbol{S} \geq \boldsymbol{0}, \ \boldsymbol{1}^\top \boldsymbol{S} = \boldsymbol{1}^\top, \ \boldsymbol{C} \geq \boldsymbol{0}, \ \boldsymbol{E} \geq \boldsymbol{0}, \tag{8c}$$

$$\boldsymbol{E}_p \in \mathcal{B}_{\text{LR}}, \ p = 1, \ldots, R(R-1)/2, \tag{8d}$$

where $\theta_1, \theta_2 \geq 0$ are regularization parameters, and the sets $\mathcal{A}_{\text{LR}}$ and $\mathcal{B}_{\text{LR}}$ are used for adding the low-rank constraints onto $\boldsymbol{S}_r$ and $\boldsymbol{E}_p$, respectively, which will be stated later. The nonnegativity constraints are added to reflect the physical meaning of the factors. The regularization $\varphi(\cdot)$ is used to exploit the sparsity of the abundances that is often observed in the literature [19]–[22]. The regularization has the form of $\varphi(\boldsymbol{X}) = \sum\sum([\boldsymbol{X}]_{i,j}^2 + \varepsilon)^{\frac{q}{2}}$ with $0 < q \leq 1$ and $\varepsilon > 0$, which is often used as a non-convex sparsity promoter in the literature; see, e.g., [23].

B. Algorithm Design

We propose an inexact block coordinate descent algorithm to tackle Problem (8).

1) Solver for Updating $\boldsymbol{C}$: To begin with, we update each element in $\boldsymbol{C}$ by

$$c_{kr} \leftarrow \max\left(\frac{\tilde{\boldsymbol{y}}_{kr} \tilde{\boldsymbol{s}}_{kr}^\top}{\|\tilde{\boldsymbol{s}}_{kr}\|_2^2},\ 0 \right), \tag{9}$$

$$k = 1, \ldots, K, r = 1, \ldots, R,$$

where

$$\tilde{\boldsymbol{s}}_{kr} = \boldsymbol{S}(r,:) + \sum_{a=1, a \neq r}^{R} c_{ka} \boldsymbol{e}_{ka}, \tag{10}$$

$$\tilde{\boldsymbol{y}}_{kr} = \boldsymbol{Y}(k,:) - \sum_{\substack{a=1 \\ a \neq r}}^{R} c_{ka} \boldsymbol{S}(a,:) - \sum_{\substack{a=1 \\ a \neq r}}^{R-1} \sum_{\substack{m=a+1 \\ a \neq r}}^{R} c_{ka} c_{km} \boldsymbol{e}_{am},$$

where $\boldsymbol{e}_{ka}$ denotes the $1 \times IJ$ row abundance vector associated with the mixture of endmembers k and a for all pixels. The update is derived following the classic update in the HALS algorithm for NMF; see [24].

2) Solver for Updating $\boldsymbol{S}$: For the $\boldsymbol{S}$-subproblem, we use the following gradient projection (GP) operator:

$$\boldsymbol{S}^{(t+1)} \leftarrow \text{Proj}_{\mathcal{S}}\left(\boldsymbol{S}^{(t)} - \beta^{(t)} \boldsymbol{G}_{\boldsymbol{S}}^{(t)} \right), \tag{11}$$

where the notation $\text{Proj}_{\mathcal{S}}(\cdot)$ is the projector on the set $\mathcal{S}$, $\boldsymbol{G}_{\boldsymbol{S}}^{(t)}$ denotes the gradient w.r.t. $\boldsymbol{S}$ at t-th iteration, $\beta^{(t)}$ is the step size, and the set $\mathcal{S} \subseteq \mathbb{R}^{R \times IJ}$ is defined as

$$\mathcal{S} = \{\boldsymbol{S} | \boldsymbol{S} \geq \boldsymbol{0}, \boldsymbol{1}^\top \boldsymbol{S} = \boldsymbol{1}^\top, \boldsymbol{S}_r \in \mathcal{A}_{\text{LR}}, \ r = 1, \ldots, R\}. \tag{12}$$

The challenge is that there is no tractable solution designed for the GP in (11). Here, we use the *alternating projection* (AP) operator proposed in [16]. The solver expresses $\mathcal{A}_{\text{LR}} = \{\boldsymbol{S}_r \in \mathbb{R}^{I \times J} | \|\boldsymbol{S}_r\|_* \leq \widetilde{L}\}$ and alternates projection over $\mathcal{A}_{\text{LR}}$ and the simplex constraint $\mathcal{A}_{\text{splx}} = \{\boldsymbol{S} \in \mathbb{R}^{R \times IJ} \mid \boldsymbol{1}^\top \boldsymbol{S} = \boldsymbol{1}^\top, \ \boldsymbol{S} \geq \boldsymbol{0}\}$. The algorithm often converges very quickly; see details in [16].

3) Solver for Updating $\boldsymbol{E}$: For $\boldsymbol{E}$-subproblem, we also use the GP method:

$$\boldsymbol{E}^{(t+1)} \leftarrow \text{Proj}_{\mathcal{E}}\left(\boldsymbol{E}^{(t)} - \eta^{(t)} \boldsymbol{G}_{\boldsymbol{E}}^{(t)} \right), \tag{13}$$

where $\eta^{(t)}$ and $\boldsymbol{G}_{\boldsymbol{E}}^{(t)}$ respectively denote the step size and gradient used at t-th iteration, $\text{Proj}_{\mathcal{E}}(\cdot)$ denotes the projector on the set $\mathcal{E} = \{\boldsymbol{E} \in \mathbb{R}^{P \times IJ} | \boldsymbol{E} \geq \boldsymbol{0}, \boldsymbol{E}_p \in \mathcal{B}_{\text{LR}}, \ p = 1, \ldots, P\}$. Following the algorithm for the $\boldsymbol{S}$-update, the projection is computed using a similar alternating projection procedure.

Our overall algorithm involves (9), (11), and (13), where the solvers for (11) and (13) leverage the AP-based solvers in [16]. This algorithm is named as *bilinear gradient projection alternating projection algorithm* (BiGradPAPA). Note that the Nesterov's extrapolation technique is adopted in our implementation for updating $\boldsymbol{S}$ and $\boldsymbol{E}$, following that in [17].
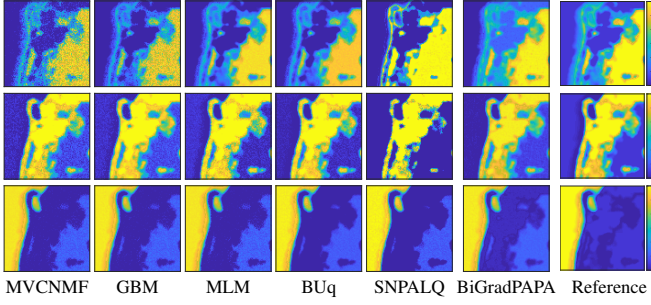
Fig. 3. The estimated linear abundance maps of Samson data by different methods. From top to bottom: `Soil`, `Tree`, and `Water`.

Methods	MSE of C	MSE of S	MSE of E	Time (min.)
MVCNMF	0.0100 ± 0.0003	0.0216 ± 0.0003	—	1.30 ± 0.02
GBM	—	0.0148 ± 0.0002	0.999 ± 0.0068	0.96 ± 0.04
MLM	—	0.0138 ± 0.0003	—	0.56 ± 0.02
BUq	0.0142 ± 0.0003	0.0134 ± 0.0003	0.9968 ± 0.0082	2.21 ± 0.11
SNPALQ	0.0398 ± 0.0021	0.0803 ± 0.0057	1.5370 ± 0.0736	$\mathbf{0.05 \pm 0.04}$
BiGradPAPA	$\mathbf{0.0058 \pm 0.0001}$	$\mathbf{0.0113 \pm 0.0003}$	$\mathbf{0.2300 \pm 0.0018}$	0.44 ± 0.03

IV. EXPERIMENTS

We compare our method with a number of SOTA baselines, including MVCNMF [25], GBM [5], MLM [7], BUq [26], and SNPALQ [10]. The method MVCNMF is designed for LMM-based HU, and GBM, MLM, BUq, and SNPALQ are the methods for BMM-based HU. Note that for the methods GBM and MLM, we first produce the endmember spectral signatures determined by MVCNMF [25], and then perform these methods to estimate the abundance maps. In the AP solvers for updating S and E, we stop the iteration when the relative change of the iterates of the latent factors is smaller than 10^{-3}. All algorithms are terminated when the relative change of the objective value is smaller than 5×10^{-5}. In the semi-real data experiments, we mainly use the *mean squared error* (MSE) [27] of C, S, and E as the performance metric.

A. Semi-Real Experiment

We generate the bilinear semi-real HSI data following Eq. (3). The zero-mean white Gaussian noise with SNR=40dB is added to the HSI data. The dataset we used is a subsence of the Samson data, which is obtained by Florida Environment Research Institute using Samson sensor. The used subimage contains 95×95 pixels and 156 bands. This subimage contains three endmembers: `Soil`, `Tree`, and `Water`.

From Table I, one can see that the proposed method achieves the best over the MSE metric. Fig. 3 shows the estimated linear abundance maps. One can observe that the results obtained by baselines contain undesired noise. Fig. 4 compares the interaction abundance maps obtained by MVCNMF+GBM, BUq, SNPALQ, and the proposed method. One can see that our method exhibits the most promising performance. The spectral signatures obtained by the proposed BiGradPAPA are much closer to the ground-truth, see Fig. 5.
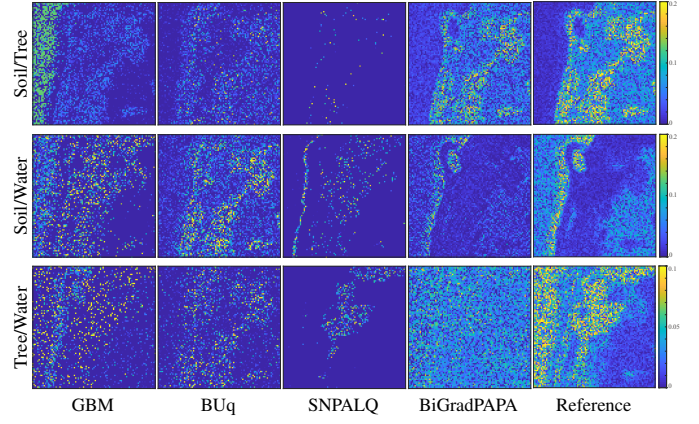

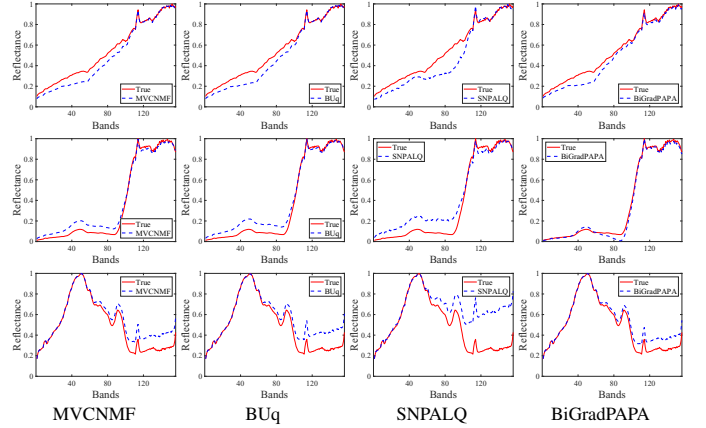Fig. 4. The estimated bilinear abundance maps of Samson data by different methods.

Fig. 5. The estimated spectral signatures of Samson data by different methods. From top to bottom: `Soil`, `Tree`, and `Water`.

B. Real-Data Experiment

We also test baselines on real HSI unmixing task. An subimage of AVIRIS HSI data with 50×50 pixels and 181 bands (after removing low SNR bands), covered over Moffett Field, is used. The subimage has been wildly studied in HU researches, which mainly contains three endmembers, including `Soil`, `Vegetation`, and `Water`.

Figs. 6 and 7 show the estimated S_r's and E_p's, respectively. One can see that all methods produce similar S_r's. However, the proposed method obtains slightly clearer boundaries (e.g. the map of `Vegetation`), and keeps the smooth region of the map for `Soil` better than the ones obtained using the baselines. All methods can identify the bilinear interactions between `Soil` and `Vegetation` in the coastal area. BiGradPAPA and BUq obtain the similar bilinear abundances between `Soil`/`Water` and `Vegetation`/`Water`, while BiGradPAPA's result has better continuity of the boundary.

V. CONCLUSION

In this work, we proposed a new algorithm for HU under the BMM. Our HU criterion is formulated from an LL1 tensor decomposition perspective. Unlike prior works that often need stringent conditions to ensure the identifiability of the
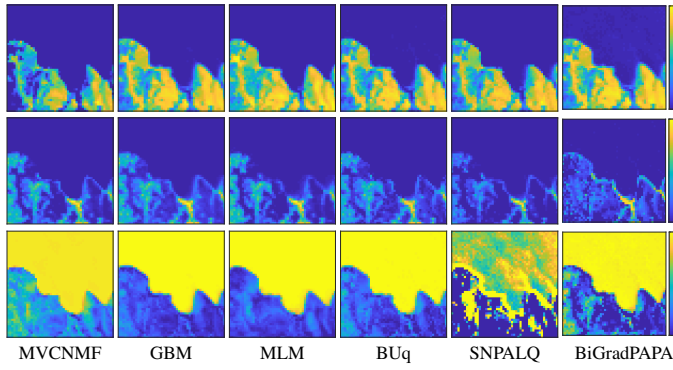
Fig. 6. The estimated S_r's of the Moffett data by different methods. From top to bottom: `Soil`, `Vegetation`, and `Water`.
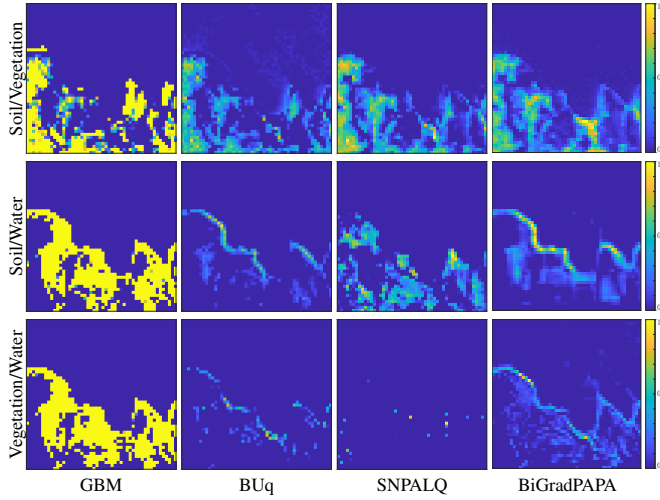

Fig. 7. The estimated E_p's of the Moffett data by different methods.

endmembers and abundances, model identification is naturally guaranteed by the `LL1` tensor's essential uniqueness under mild conditions. We proposed a block coordinate descent algorithm to tackle the formulated HU criterion. The algorithm is designed to effectively handle a series of constraints and regularization arising in the context of BMM-HU. We tested the algorithm over a series of semi-real and real experiments and observed promising results.

REFERENCES

[1] J. M. Bioucas-Dias, A. Plaza, N. Dobigeon, M. Parente, Q. Du, P. Gader, and J. Chanussot, "Hyperspectral unmixing overview: Geometrical, statistical, and sparse regression-based approaches," *IEEE J. Sel. Topics Appl. Earth Observ. Remote Sens.*, vol. 5, no. 2, pp. 354–379, 2012.

[2] W.-K. Ma, J. M. Bioucas-Dias, T. Chan, N. Gillis, P. Gader, A. J. Plaza, A. Ambikapathi, and C. Chi, "A signal processing perspective on hyperspectral unmixing: Insights from remote sensing," *IEEE Signal Process. Mag.*, vol. 31, no. 1, pp. 67–81, 2014.

[3] N. Dobigeon, J.-Y. Tourneret, C. Richard, J. C. M. Bermudez, S. McLaughlin, and A. O. Hero, "Nonlinear unmixing of hyperspectral images: Models and algorithms," *IEEE Signal Process. Mag.*, vol. 31, no. 1, pp. 82–94, 2014.

[4] W. Fan, B. Hu, J. Miller, and M. Li, "Comparative study between a new nonlinear model and common linear model for analysing laboratory simulated-forest hyperspectral data," *IEEE Trans. Geosci. Remote Sens.*, vol. 30, no. 11, pp. 2951–2962, 2009.

[5] A. Halimi, Y. Altmann, N. Dobigeon, and J.-Y. Tourneret, "Nonlinear unmixing of hyperspectral images using a generalized bilinear model," *IEEE Trans. Geosci. Remote Sens.*, vol. 49, no. 11, pp. 4153–4162, 2011.

[6] Y. Altmann, A. Halimi, N. Dobigeon, and J.-Y. Tourneret, "Supervised nonlinear spectral unmixing using a postnonlinear mixing model for hyperspectral imagery," *IEEE Trans. Image Process.*, vol. 21, no. 6, pp. 3017–3025, 2012.

[7] R. Heylen and P. Scheunders, "A multilinear mixing model for nonlinear spectral unmixing," *IEEE Trans. Geosci. Remote Sens.*, vol. 54, no. 1, pp. 240–251, 2016.

[8] Q. Wei, M. Chen, J.-Y. Tourneret, and S. Godsill, "Unsupervised nonlinear spectral unmixing based on a multilinear mixing model," *IEEE Trans. Geosci. Remote Sens.*, vol. 55, no. 8, pp. 4534–4544, 2017.

[9] Y. Deville, "From separability/identifiability properties of bilinear and linear-quadratic mixture matrix factorization to factorization algorithms," *Digit. Signal Process.*, vol. 87, pp. 21–33, 2019.

[10] C. Kervazo, N. Gillis, and N. Dobigeon, "Provably robust blind source separation of linear-quadratic near-separable mixtures," *SIAM J. Imaging Sci.*, vol. 14, no. 4, pp. 1848–1889, 2021.

[11] R. Heylen, M. Parente, and P. Gader, "A review of nonlinear hyperspectral unmixing methods," *IEEE J. Sel. Topics Appl. Earth Observ. Remote Sens.*, vol. 7, no. 6, pp. 1844–1868, 2014.

[12] X. Fu, W.-K. Ma, T.-H. Chan, and J. M. Bioucas-Dias, "Self-dictionary sparse regression for hyperspectral unmixing: Greedy pursuit and pure pixel search are related," *IEEE J. Sel. Topics Signal Process.*, vol. 9, no. 6, pp. 1128–1141, 2015.

[13] T.-H. Chan, W.-K. Ma, A. Ambikapathi, and C.-Y. Chi, "A simplex volume maximization framework for hyperspectral endmember extraction," *IEEE Trans. Geosci. Remote Sens.*, vol. 49, no. 11, pp. 4177–4193, 2011.

[14] L. De Lathauwer, "Decompositions of a higher-order tensor in block terms—Part II: Definitions and uniqueness," *SIAM J. Matrix Anal. Appl.*, vol. 30, no. 3, pp. 1033–1066, 2008.

[15] Y. Qian, F. Xiong, S. Zeng, J. Zhou, and Y. Y. Tang, "Matrix-vector nonnegative tensor factorization for blind unmixing of hyperspectral imagery," *IEEE Trans. Geosci. Remote Sens.*, vol. 55, no. 3, pp. 1776–1792, 2017.

[16] M. Ding, X. Fu, and X.-L. Zhao, "Fast and structured block-term tensor decomposition for hyperspectral unmixing," *IEEE J. Sel. Topics Appl. Earth Observ. Remote Sens.*, vol. 16, pp. 1691–1709, 2023.

[17] M. Ding, X. Fu, T.-Z. Huang, J. Wang, and X.-L. Zhao, "Hyperspectral super-resolution via interpretable block-term tensor modeling," *IEEE J. Sel. Topics Signal Process.*, vol. 15, no. 3, pp. 641–656, 2021.

[18] G. Zhang, X. Fu, J. Wang, X.-L. Zhao, and M. Hong, "Spectrum cartography via coupled block-term tensor decomposition," *IEEE Trans. Signal Process.*, vol. 68, pp. 3660–3675, 2020.

[19] M.-D. Iordache, J. M. Bioucas-Dias, and A. Plaza, "Sparse unmixing of hyperspectral data," *IEEE Trans. Geosci. Remote Sens.*, vol. 49, no. 6, pp. 2014–2039, 2011.

[20] J. Sigurdsson, M. O. Ulfarsson, and J. R. Sveinsson, "Hyperspectral unmixing with l_q regularization," *IEEE Trans. Geosci. Remote Sens.*, vol. 52, no. 11, pp. 6793–6806, 2014.

[21] P. V. Giampouras, K. E. Themelis, A. A. Rontogiannis, and K. D. Koutroumbas, "Simultaneously sparse and low-rank abundance matrix estimation for hyperspectral image unmixing," *IEEE Trans. Geosci. Remote Sens.*, vol. 54, no. 8, pp. 4775–4789, 2016.

[22] M.-D. Iordache, J. M. Bioucas-Dias, and A. Plaza, "Collaborative sparse regression for hyperspectral unmixing," *IEEE Trans. Geosci. Remote Sens.*, vol. 52, no. 1, pp. 341–354, 2014.

[23] X. Fu, W.-K. Ma, J. M. Bioucas-Dias, and T.-H. Chan, "Semiblind hyperspectral unmixing in the presence of spectral library mismatches," *IEEE Trans. Geosci. Remote Sens.*, vol. 54, no. 9, pp. 5171–5184, 2016.

[24] A. Cichocki, R. Zdunek, and S. Amari, "Hierarchical ALS algorithms for nonnegative matrix and 3d tensor factorization," in *Independent Component Analysis and Signal Separation*, 2007, pp. 169–176.

[25] L. Miao and H. Qi, "Endmember extraction from highly mixed data using minimum volume constrained nonnegative matrix factorization," *IEEE Trans. Geosci. Remote Sens.*, vol. 45, no. 3, pp. 765–777, 2007.

[26] J. Sigurdsson, M. O. Ulfarsson, and J. R. Sveinsson, "Blind sparse nonlinear hyperspectral unmixing using an ℓ_q penalty," *IEEE Geosci. Remote Sens. Lett.*, vol. 15, no. 12, pp. 1907–1911, 2018.

[27] X. Fu, K. Huang, B. Yang, W.-K. Ma, and N. D. Sidiropoulos, "Robust volume minimization-based matrix factorization for remote sensing and document clustering," *IEEE Trans. Signal Process.*, vol. 64, no. 23, pp. 6254–6268, 2016.